Journal of Micro and Bio Robotics (2024) 20:8
https://doi.org/10.1007/s12213-024-00173-0

RESEARCH

Flow measurement in microfluidic chips through optical trapping and deep learning

Nicolas Inacio[1] · Edison Gerena[1] · Ferhat Sadak[1,2] · Sinan Haliyo[1]

Received: 2 February 2024 / Revised: 28 June 2024 / Accepted: 1 July 2024 / Published online: 11 July 2024

Abstract
Mechanobiology is an emerging multidisciplinary field that involves the study of the mechanisms by which biological organisms sense and respond to mechanical stimuli. In recent years, this field has seen significant advancements through the application of microfluidics and optical manipulation. Microfluidics enables precise control of channel content and flow with great precision, while optical trapping allow for manipulation of microscopic objects. Combining these disciplines offers new opportunities for studying biological phenomena with reduced scale experiments. However, challenges remain in coordinating microfluidics with optical manipulation within confined spaces, in particular when working with biological entities. To address these limitations, an integrated approach is proposed, using 3D optical manipulation setup, microfluidics and deep learning image recognition to estimate forces experienced by optically trapped objects. By analyzing the bead's displacement within the flow, forces are quantified using a deep learning algorithm. Experimental results demonstrate force variations based on the position within the chip, revealing the potential for improved understanding of biological mechanisms through characterization of local forces. This study facilitates the establishment of optofluidics manipulations, paving the way for future explorations in mechanobiology.

Keywords Microfluidics · Optical tweezers · Optofluidics · Deep learning · Force estimation · Microscopic manipulation

1 Introduction

For the past few years, there has been rapid evolution in the mechanobiology field. Studying certain biological processes through the lens of mechanics has led to advancements in the understanding of these mechanisms [1, 2], something nearly impossible with conventional experiments, that require analysis on large samples at the scale of a cell population for instance.

In addressing the inherent challenges associated with such investigations, numerous studies have embraced the integration of microfluidic technologies [2]. Microfluidics enables the creation of structures comprising channels and chambers. The manipulation of content within these structures is facilitated by regulating internal flows through the utilization of pressure controllers. Consequently, it becomes feasible to alter the medium within the chip, to pass microparticles through the channels, and even to allow cells to pass through if the width permits. Overall, this offers the possibility of miniaturizing certain classical experiments on a micrometer scale platform [3–5].

Conversely, optical manipulation has become a highly coveted research field for biology, since the work of Arthur Ashkin formulated the principle of optical tweezers in 1986 [6, 7]. By using the radiation pressure applied by a laser beam, microparticles, microscopic objects, or cells can be held in an optical trap [8, 9], even micro-robots [10]. Optical tweezers have demonstrated their relevance in analyzing behaviors

Edison Gerena, Ferhat Sadak and Sinan Haliyo contributed equally to this work.

✉ Nicolas Inacio
nicolas.inacio@isir.upmc.fr

Edison Gerena
edison.gerena@isir.upmc.fr

Ferhat Sadak
fsadak@bartin.edu.tr

Sinan Haliyo
sinan.haliyo@sorbonne-universite.fr

[1] Institut des Systèmes Intelligents et de Robotique (ISIR), CNRS UMR 7222, Sorbonne Université, 4 place Jussieu, Paris 75005, France

[2] Department of Mechanical Engineering, Bartin Technical University, Bartin 74100, Turkey

in the microscopic world, particularly in the microbiological realm [2, 9]. Furthermore, optical forces on trapped spherical objects can be modelled linearly, as the restoring optical force is proportional to the distance from its equilibrium position [11]. This particularity has led to the use of optical trapping also for quantitative force measurements [12], such as the strength of inter-molecular bonds [13] or the stiffness of a cell membrane [14], and to the development of optical tweezers with haptic feedback [15, 16].

The convergence of microfluidics and optical manipulation, denoted as optofluidics, has introduced a paradigm wherein microparticles are optically manipulated within a microfluidic chip. Through this, it becomes possible to replicate biological experiments on a reduced scale, with the ability to sort, select, or differentiate microscopic objects, as these methods would surpass the actual limitations posed by manual experimentation [1, 17–19]. It is now possible to have access to a confined microscopic space for studying biological phenomena using tools such as optical tweezers. For instance, there is an experiment that enables the sorting of cells based on their fluorescence response to mechanical stress [20], proposing an approach to cellular biomechanics using optofluidics.

However, [21] indicates that one limitation of these experiments lies in the coordination between microfluidics and optical tweezers. For instance, some applications involve automating the movement of the optical trap along a predefined trajectory [22]. Conversely, the measurement of flow force on a biological object in microfluidics has been observed [1], but the optical trap remains stationary, and cells are passed in front of the trap using the flow in the chip.

Another limitation in the field of optofluidics, as mentioned by Zhu et. al [21], is the freedom of movement in three dimensions. Especially in biology, numerous mechanisms are governed by the structure of the biological elements involved [23]. The possibility of interacting with these elements with non-static optical tweezers in different spatial conformations would undoubtedly bring new insights for mechanobiology. Optical manipulation has already demonstrate 3D manipulation capabilities [24, 25]. Therefore, there is a progressively advancing exploration of mechanobiology utilizing optofluidics, accompanied by a growing demand for precision and comprehension of local forces involved at the microbiological scale, in particular applied to the biological studied entities. For various applications, such as lab-on-chip organs, it is a main problematic to enhance our comprehension of the roles played by fluidic forces on biological objects within a microfluidic chip.

With the aim of enhancing the synergy between microfluidics and optical trapping techniques, this paper introduced the integration of optofluidics and deep learning. Utilizing a specially designed optical tweezer system and a deep learning algorithm, this approach facilitates the manipulation of microscopic objects in three dimensions within a microfluidic sample. The force's behavior of the manipulated objects in the flow of a microfluidic channel is analyzed, in the attempt to address the previous problematic.

The flow imposed by a circulating medium within a microfluidic chip is significantly constraint by the walls and the chip design. The focus here is to investigate how the displacement of a polystyrene bead varies based on its position in the microfluidic chip. A series of experiments that allows to measure the drag force at different pressures are performed. The displacement of this sphere around the origin point of the laser is monitored within the microfluidic flow, and associated to a force thanks to the deep learning to show how it is possible to measure the flow force locally. The objective of this study is, by estimating the force experienced by optically captured objects, to prove the relevance of an optofluidic trapping device with image recognition based in deep learning to characterize the mechanical flow inside the chip, and pave the way for more complex mechano-biology experiments.

2 Methodology

2.1 Microfluidics

For microfluidic control, a commercial flow controller is used (OB1 MK4, Elveflow®). The software provided allows to manage the different pressures applied. In the setup, two pressure channels are used from the controller—one for the input and the other for the output of the microfluidic chip, which consists of a simple straight-line path. The pressure in the main channel of the chip is calculated based on the difference from the pressure where the flow is static in the channel. At the input of the chip, an Safe-Lock Eppendorf®tube is placed containing a solution of 3 µm polystyrene beads. At the output, another tube serves as a waste collection container for the medium passing through the microfluidic chip.

The microfluidic chips themselves are meticulously crafted from Polydimethylsiloxane (PDMS) through a molding process involving silicon wafers. The selection of PDMS as the material for our microfluidic chips stems from several advantageous characteristics. Firstly, PDMS's transparency to light enables optimal manipulation of objects within the microfluidic chip, facilitating precise experimental control. Secondly, its flexibility and ease of manipulation make it a practical choice for the fabrication of intricate microfluidic structures. PDMS is also a well-established material in similar experimental contexts, boasting a comprehensive documentation that proves invaluable in troubleshooting potential issues. Given our future endeavors in mechanobiology experiments using this system, the material's biocompatibility is paramount [26]. Furthermore, PDMS's transparency to gases

is crucial for facilitating the circulation of gases between the interior and exterior of the chip [27]. This property becomes significant as we plan to employ an incubator to maintain cells in a favorable environment with controlled levels of CO2 and N2 [28].

The microfluidic patterns incorporated into the chips consist of channels with a width of 40 µm. The PDMS compound, constituting a mixture of 30g of PDMS and 3g of cross-linking agent for each wafer, underwent a meticulous de-bubbling process utilizing a vacuum pump. Subsequent to ensuring the PDMS adhered to the wafer, the assembly was subjected to an oven at 65°C for a duration of 4 hours. Following the extraction of PDMS from the mold, the desired microfluidic patterns were delineated, and apertures were introduced at the input and output locations. The region of interest was then affixed to a slender glass slide using a plasma cleaner for 2 minutes, followed by a thorough wash with isopropanol. The final structure underwent additional consolidation in an oven set at 90°C for 20 minutes (see the fabrication process on the Fig. 2). Microfluidic connections were established through the incorporation of fine tubing directed towards the tubes and the pressure controller, completing the microfluidic system.

2.2 Optical manipulation

The system is identified in Fig. 1. To conduct the experiments, a customized optical path is set up to trigger the trapping within a Petri dish containing the sample [10]. As source, an infrared laser (1064 nm, minimum power: 100mW, maximum power: 10W, typical power: 300 mW) is used. The laser beam then passes through a series of lenses and mirrors, including a galvanometer, to control the final focus point's position in three dimensions. Finally, the beam passes through an oil-immersion microscope objective (Olympus UPlanFLN, 40x magnification) to deliver the laser beam into the sample. The image formed within the sample is captured by a CMOS camera (640 × 640 pixels) with a total magnification of x4000, positioned parallel to the first optical path. The images are processed using custom-coded software designed for this system.

The activation and movement of the optical tweezers are achieved through teleoperation using a joystick. This allows for movements in six degrees of freedom (three translations and three rotations) in a three-dimensional space to control one or several focal points of the optical tweezers, enabling the manipulation of spheres or even more complex structures within a region of 100 μm width in the X/Y plan. The microscope objective is strategically positioned from beneath, directed towards the sample earmarked for observation or manipulation. It remains fixed, with the sample constituting the mobile component during adjustments. To facilitate this, the Petri dish designated for manipulated objects is situated on two superimposed platforms: a microstage and a nanostage.

A stage-top live cell incubator system (Incubator T Series, Live Cell Instruments LCI) is employed in our experimental setup, positioned around the platform where our samples are situated for optical trapping. This enclosed space is connected to CO2 and N2 sources, features precise temperature control, and incorporates a humidifier to maintain humidity levels above 90%. By configuring this confined environment, an exceptionally conducive setting for the biological entities under study is established. This not only allows for the creation of an optimal environment but also ensures a constant temperature throughout our microfluidic experiments, enhancing experimental precision.

2.3 Particle tracking through deep learning

In this study, the YOLOv7 algorithm is employed to develop and evaluate a micro-bead displacement measurement tech-

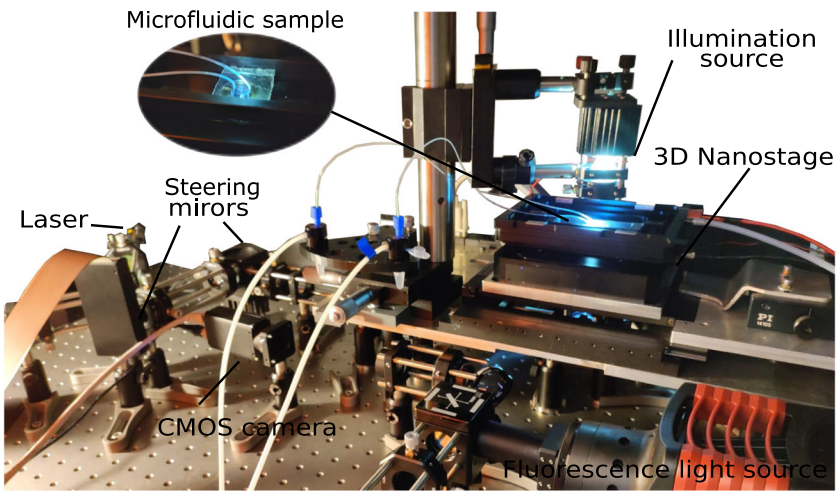

Fig. 1 Image of the optical trapping system and the microfluidic set-up

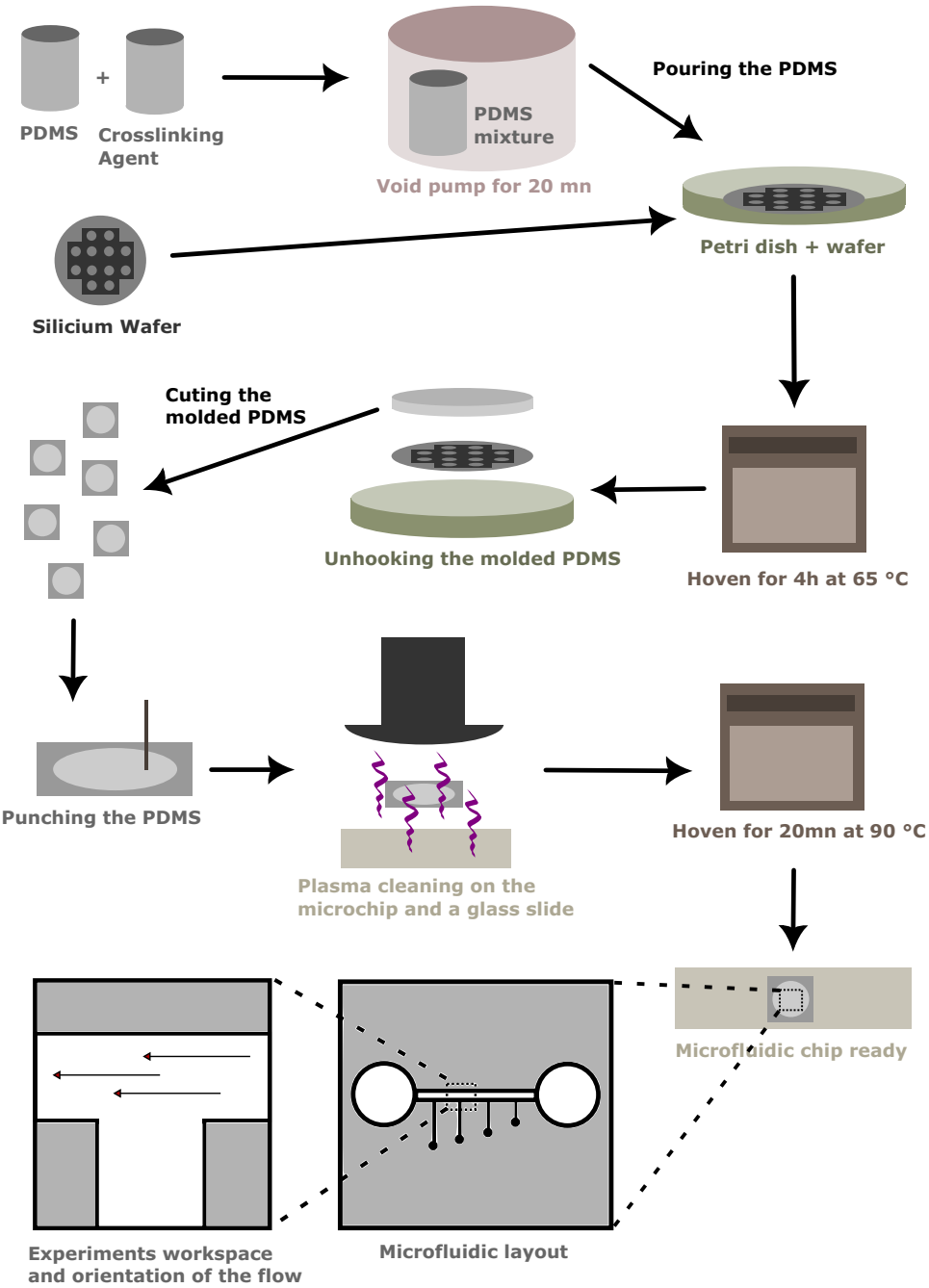

Fig. 2 Fabrication process of the PDMS microfluidic chip. Red arrows indicate the direction of the flow, mainly contained in the main central channel

nique [29]. In order to achieve this, a dataset of 500 micro-bead images is used, divided into training, validation, and testing sets. The images were resized to 640 × 640 pixels before algorithm training. The resolution of the micro-bead tracking algorithm is about 100 nanometer which allows us to precisely track the micro-bead displacement to measure the force required. In this section, a brief description of the YOLOv7 architecture will be provided.

YOLOv7 is composed of the following parts: Cross-Batch Stabilization (CBS), E-ELAN, and MaxPool-1 (MP1). Convolutional operations, batch normalization, and SiLU activation functions are all included in the CBS component, allowing for effective feature extraction. While keeping the ELAN structure, the E-ELAN module improves learning capabilities by directing various computing units in charge of feature extraction to learn a wider range of features, maintaining the initial gradient path. The MP1 structure integrates pooling and convolution, which are two distinct down-sampling techniques. This amalgamation enables the network to autonomously determine the most suitable down-sampling approach based on the prevailing contextual considerations.

The YOLOv7 model's head, constructed with the Feature Pyramid Network (FPN) architecture incorporating PANet integration, assumes a critical role in the overall architecture. It incorporates multiple Convolutional, Batch Normalization, and SiLU activation (CBS) blocks. The head also includes an E-ELAN, a MaxPool-2 (MP2), and a Spatial Pyramid Pooling and Convolutional Spatial Pyramid Pooling (Sppcspc) structure. By merging the Spatial Pyramid Pooling (SPP) structure and the Convolutional Spatial Pyramid (CSP) structure, the Sppcspc structure efficiently improves the network's perceptual field. The MP2 block, executing downsampling and feature extraction concurrently, closely resembles the MP1 block, with minor adjustments to the output channel count. The prediction network, consisting of the head, is the component where the final predictions are derived.

In the evaluation of YOLOv7's performance in micro-bead center location, key metrics such as box loss, objectness loss, and classification loss are measured over 100 epochs, as shown in Fig. 3. The combined YOLOv7 loss, as defined in Eq. 1, serves as a comprehensive metric to quantify the disparity between the model's predicted results and the actual data.

$$loss = l_{\text{bbox}} + l_{\text{object}} + l_{\text{classification}} \tag{1}$$

The box loss metric estimates the algorithm's effectiveness in locating the object's center and fitting the object within a predicted bounding box. Objectness quantifies the probability of identifying an object within a specific area of interest, while the classification loss assesses the accuracy of predicting the appropriate class label for the identified object.

Additionally, the metrics $mAP_{0.5}$ and $mAP_{0.5:0.95}$ evaluate the mean Average Precision (mAP) across various Intersection over Union (IoU) criteria ranging from 0.5 to 0.95. Precision and Recall, determined by the parameters true positive (TP), false positive (FP), true negative (TN), and false negative (FN), are employed to calculate mAP. Precision, as indicated in Eq. 2, measures the percentage of positive identifications that are correct.

$$Precision = \frac{TP}{TP + FP} \tag{2}$$

Recall, as defined in Eq. 3, quantifies how many actual positive instances were correctly identified by the algorithm.

$$Recall = \frac{TP}{TP + FN} \tag{3}$$

The calculation of mAP involves utilizing the area under the precision-recall curve, as outlined in Eq. 4, to determine the average precision for each class.

$$mAP = \frac{1}{c}\Sigma_{i=1}^{c} AP_i \tag{4}$$

Intersection over Union (IoU), expressed in Eq. 5, measures the extent to which the predicted bounding box overlaps with the ground-truth bounding box.

$$IoU = \frac{\text{Area of Overlap}}{\text{Area of Union}} \tag{5}$$

Moreover, YOLOv7 serves as the foundational model for micro-bead detection, providing bounding box information in the form of (x, y, w, h), where x and y denote the center position of the detected bounding box, while w and h represent its width and height. In the experimental setup, the micro-bead exhibits no motion at the conclusion of the experiments under various environmental conditions. This information is utilized to ascertain the positional displacement of the micro-bead in the x and y axes. A low-pass filter is subsequently applied to retain pertinent information. The force affecting the micro-bead is then predicted using the

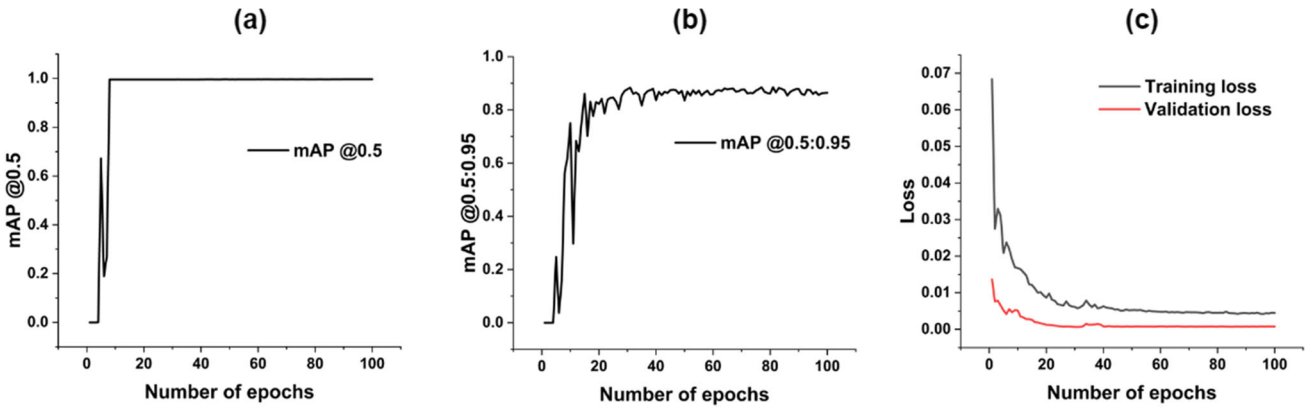

Fig. 3 Performance evaluation of YOLOv7 model for 100 epochs based on: **(a)** mAP@0.5 **(b)** mAP@0.5:0.95 **(c)** Training and validation loss for YOLOv7

optical force model [30].

$$F_{flow} = K \cdot (X_{laser} - X_{probe}) \tag{6}$$

Here, $X_{laser} - X_{probe}$ represents the displacement between the origin position of the bead (corresponding to the laser position) and the actual bead position, calculated through the deep learning method. K denotes the stiffness of the trap.

The experimental procedure for measuring stiffness is the opposite of the one employed in this article, and is obtained through the Drag Force method [31], using the Eq. 7. In real-time or through video observation, a sphere with a given radius r is trapped in a medium with a specified viscosity η, and it is displaced with large movements to induce a shift of the sphere from the presumed center of the optical trap. The speed of this movement is noted v. This displacement is indicative of the trap stiffness, and the restoring force within the trap is equivalent to the drag force exerted by the medium surrounding the sphere. This assumption is made under the consideration that the drag force is the sole opposing force to the optical trap. The calculation of stiffness K is rapid, yielding results dependent on the direction (X or Y) and laser power, with increased stiffness observed as laser power is augmented. Measurement of stiffness in the Z-direction is not undertaken, as such displacements are not of relevance in this context. The values of stiffness that will be used in this paper are presented in Table 1.

$$F_{drag} = 6\pi\eta r v \tag{7}$$

2.4 Experimental protocol

Five distinct experiments have been executed, each capturing the behavior of a polystyrene bead within the microfluidic flow. Each experiment corresponds to a unique pressure or laser power setting, dictating the strength of the optical trap applied to the sphere.

The input and output pressures were initially configured at 300 mbar. Subsequently, the input pressure is systematically adjusted to attain a state of static flow, identified by the immobility of the spheres that previously moved within the channel. In each experiment, the input pressure is subsequently varied from this established static flow value to successively achieve several pressure levels: 0.30 mbar, 0.80 mbar, and 1.80 mbar difference between the static flow and the measurement flow.

Table 1 Stiffness of the optical trap

Laser power	X	Y
0.75 W	54.3 pN/µm	52.4 pN/µm
0.95 W	67.2 pN/µm	65.4 pN/µm

Before each measurement, the optical tweezers are activated to trap one of the spheres passing through the channel. With the flow activated by the pressure difference, 8 different positions are used to stop the bead, starting from the wall and moving towards the chamber as show in Fig. 5.(f). Each position is spaced by 10 µm, achieved by displacing the platform supporting the sample, controlled by the optical tweezers software. The speed at which the bead is moved between each of these points is 10 µm/s. The stop at each position lasts for 30 seconds — except for Fig. 5.(c) where the first position is at 15 seconds. The laser power will be adjusted to 0.95 W or 0.75 W depending on the experiment. The experiments were recorded at 64 frames per second (fps) to optimize image recognition.

3 Results and discussion

3.1 Micro-bead tracking evaluation

Training results are primarily evaluated using the mAP@0.5, mAP@0.5:0.95, and training and validation loss over 100 epochs, as shown in Fig. 3. The training process has been executed on analogous experiments wherein the polystyrene bead remains stationary within the microfluidic chamber. The validation loss serves as an indicator of the model's generalization to new data, elucidating its performance on previously unseen information. Conversely, the training loss gauges the model's efficacy in learning from the provided training data. As a result, the YOLOv7 model's training and validation losses exhibited a good fit for both the training and validation datasets. The model provided 100% mAP@0.5 and 87% mAP@0.5:0.95 accuracy for the detection of micro-bead for 100 epochs. To demonstrate the generalization ability of the YOLOv7 model toward micro-bead detection, 100 independent images of micro-bead are used for testing. In order to establish the model's capability for precise displacement measurement of the micro-bead, a comprehensive analysis has been conducted at various Intersection over Union (IoU) thresholds to assess accuracy. The objective is to underscore the applicability of the model for force measurement at the piconewton level. Hence, the test set was analyzed at 0.65, 0,75, 0.85, 0.95, and 1.00 IoU thresholds. As shown in Fig. 4, the model demonstrated almost 100% localization accuracy at 0.65, 0.75, 0.85 and 0.95 thresholds. On the other hand, there is a 2.4% accuracy decrease at 1.00 threshold. This error is also including the human error in ground truth data. Overall, Fig. 4 confirms the suitability of the model's localization accuracy as a base model for force measurement to provide the displacement measurement of the micro-bead at 100-nanometer resolution.

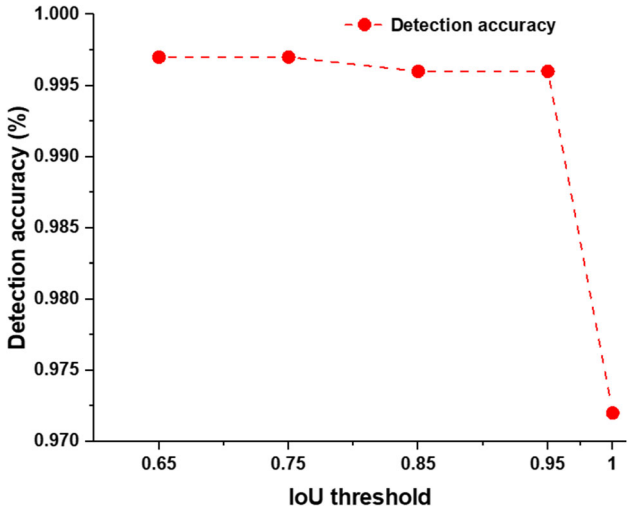

Fig. 4 Localization performance evaluation of YOLOv7 model for 100 epochs in the test set at various IoU thresholds

3.2 Experiments analysis

The position of the bead within the optical traps exhibits variations dependent on its location within the microfluidic chip—whether near a wall, at the entrance of a chamber, inside a chamber, in the middle of a channel, and forth. This behavior arises from the heterogeneity of the current velocity at these diverse locations, influencing the force exerted by the flow on the trapped object based on its operational point.

The measured force denotes the force applied to the sphere at its specific location, illustrating the impact of flow velocity on the particle. It is evident here that this force varies with the position, observed when the sphere is positioned inside the channel of a chamber where there is no flow (i.e., at the last position), resulting in a force close to 0 pN. Regardless of the applied force, the plateaus' shape remains consistent across the graphics.

Under varying pressure at the same laser power, the maximum force applied to the sphere changes from 40 pN (Fig. 5.a) to 60 pN (Fig. 5.b) and then 80 pN (Fig. 5.c), indicating a notable difference in velocity flow with increased pressure in the microfluidic chip. The force in the Y-direction is non-zero when close to the walls, while the force in the X-direction is weaker than in the main channel, owing to boundary effects. At 0.30 mbar, the pushing force in the Y-direction even surpasses that in the X-direction, showcasing the wall's influence on the sphere's movement within the current.

Furthermore, when keeping the pressure constant but varying the laser power from 0.95 W to 0.75 W (Figs. 5.a & d and .b & e), a minimal difference in force is observed,

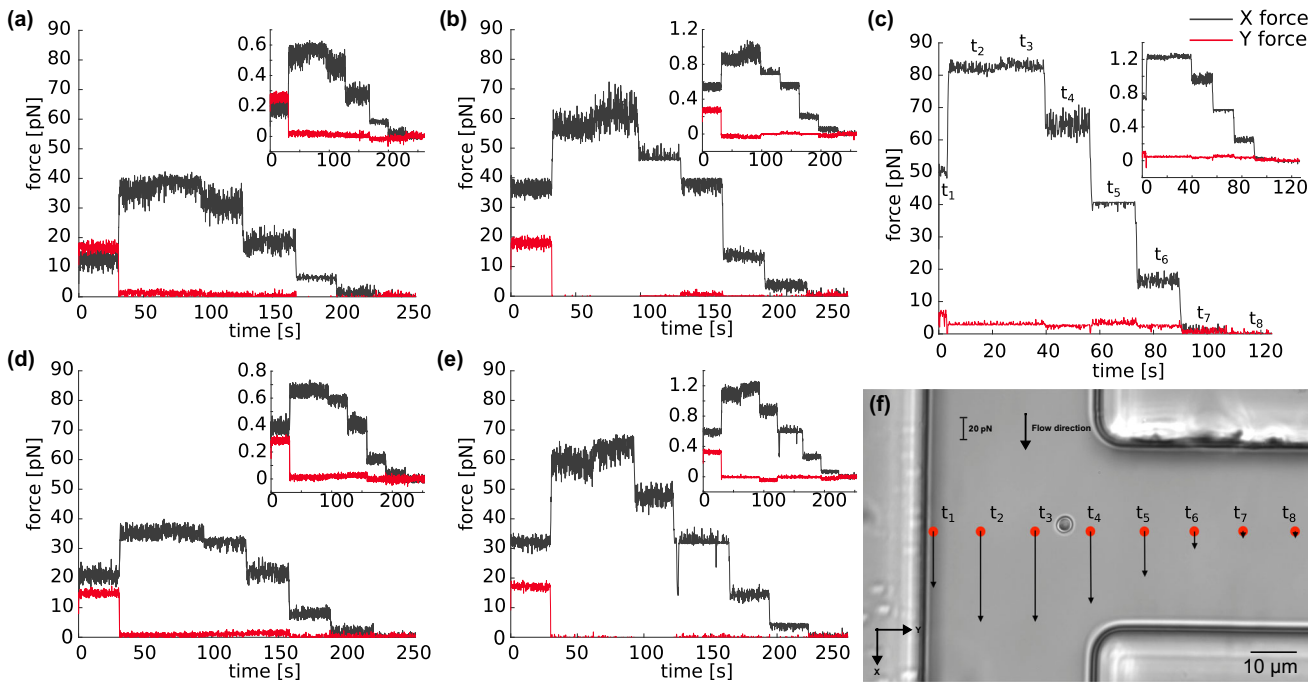

Fig. 5 Measured forces on the sphere for each experiment. (inset figures : displacement of the bead expressed in µm and seconds). Each step on the curves represents one of the 8 positions with a thirty seconds stop, as indicated in **(f)**. The experiments in graphs (a), (b), and (c) were recorded at 0.95 W. The experiments in graphs (d) and (e) were recorded at 0.75 W. **(a)**. 0.95W et 0.30 mbar. **(b)**. 0.95W et 0.80mbar. **(c)**. 0.95W et 1.80mbar. **(d)**. 0.75W et 0.30mbar. **(e)**. 0.75W et 0.80mbar. **(f)**. Representation of force vectors on the different measure spots along the channel, corresponding to the parameters set in (e)

remaining below 10 pN. This unexpected behavior may be attributed to issues with the stiffness calibration of the optical tweezers and boundary effects in the beads. It is anticipated that laser power influences the resolution and range of the measurement, with higher laser power resulting in higher stiffness and less displacement of the bead. This contradicts the expected behavior, and these small, inconsistent differences may be attributed to calibration issues and boundary effects.

When the laser power falls below 0.75 W, the sphere ceases to be trapped and becomes entrained in the flow. Conversely, at laser power exceeding 0.95 W, the sphere exhibits nearly stationary behavior, impeding precise force determination. Maintaining the laser power at approximately 1 W proves effective in retaining the sphere within the optical trap under the investigated pressures. This establishes a foundation for applying controlled pressure and forces up to 80 piconewtons, facilitating the characterization of cellular behaviors in forthcoming investigations.

One may also think about the utilization of materials other than PDMS for the fabrication of microfluidic chips. Despite its undisputed prevalence in the field of microfluidics, chosen for its numerous advantages, its applicability may be subject to scrutiny by some researchers [32]. Considerations arise, particularly concerning PDMS's low fluorescence, prompting the need for awareness of this parameter in future biological experiments [32]. Furthermore, it is reported to be transparent within the wavelength range of 240 to 1100 nm. Given our laser operates at 1064 nm, questions arise regarding potential overlap between the laser emission curves and PDMS absorption spectra. In such a scenario, careful consideration is warranted to optimize the experimental setup and ensure the efficient capture of the entire laser light. Another well-known challenge associated with PDMS is its propensity to absorb hydrophobic molecules and proteins [33] — a crucial aspect to be taken into account when dealing with these biological entities in future experiments. While other silicone-based polymers may not necessarily be deemed superior, akin to glass, they represent alternative materials worthy of contemplation for optimizing our experiments. Overall, the experiments outlined in this study exclusively utilize fluids in their liquid phase, which is the most common fluid state encountered when studying biological liquids and cellular bodies. This choice of medium was deliberate for the study at hand, with no consideration given to gas phases.

4 Conclusions and future directions

The presented system effectively allows the measurement of the force applied to a sphere in a microfluidic chip. By manually displacing the sphere within the sample, the measurement location can be precisely selected. This capability opens numerous possibilities for exploring a microscopic environment within a microfluidic chip. Then, microfluidics with optical tweezers and Deep Learning have been successfully integrated to establish an exploratory method for measuring local pushing forces within a microfluidic chip, using a polystyrene bead as a probe in this environment. This novel approach to analysis opens new avenues for future experiments conducted with these technologies, and increase the potential comprehension in applications aimed at understanding mechanobiology.

The method employed here involves data recording and Deep Learning processing of experiments after the manipulation. However, it is also possible to extend to real-time quantitative measurement of forces. This is only limited by the camera acquisition bandwidth (64 Hz), as the deep learning algorithm process time is more than 90 Hz.

Furthermore, the integration of novel image sensor types with deep learning algorithms holds the potential to enhance the bandwidth of force measurement acquisition, notably through the utilization of event-based cameras [15]. These cameras capture local changes in brightness asynchronously, pixel by pixel, allowing for the selective recording of areas exhibiting motion within the field of view. On an image scale, this effectively records only regions where movement is detected, enabling straightforward identification of object displacements. By calibrating the camera to detect a sphere, one can track the sphere's deviation from its initial position, generating real-time object position curves. Leveraging these curves in conjunction with the Drag Force Method formula facilitates the real-time determination of applied forces at high rates. Event-based cameras can be seamlessly integrated with a haptic interface or incorporated into a robotic control loop, as demonstrated by Gerena et al. in [16]. It is conceivable that such systems could be employed to establish flow control mechanisms within a microfluidic chip based on detected forces. This could prevent the flow force from surpassing a predefined threshold, safeguarding manipulated cells from excessive damage caused by the current. Additionally, such systems could be employed to set a constant flow force throughout a manipulation duration, illustrating the potential for sophisticated microfluidic control systems driven by real-time force detection.

This enhancement opens up new possibilities for applications using this system, coupling microfluidics with optical tweezers to comprehend biological mechanisms [21]. This integrated approach holds great promise in advancing the understanding of cellular and microscopic behavior and paves the way for exciting research prospects in mechanobiology.

Acknowledgements This work was supported by French National Research Agency Project Optobots (ANR-21-CE33-0003), Ile-de-France Region DIM ELICIT Projet 3BIOT, and CNRS Innovation program BIOPTIQ.

Author Contributions Co-authors contributed equally to this work.

Data Availability No datasets were generated or analysed during the current study.

Declarations

Competing interests The authors declare no competing interests.

References

1. Yao Z, Kwan CC, Poon AW (2020) An optofluidic "tweeze-and-drag" cell stretcher in a microfluidic channel. Lab Chip 20(3):601–613. https://doi.org/10.1039/C9LC01026B
2. Hu S, Ye J-y, Zhao Y, Zhu C-l (2022) Advanced optical tweezers on cell manipulation and analysis. The European Physical Journal Plus 137(9):1024. https://doi.org/10.1140/epjp/s13360-022-03190-9
3. Zhu J, Zhu X, Zuo Y, Hu X, Shi Y, Liang L, Yang Y (2019) Optofluidics: the interaction between light and flowing liquids in integrated devices. Opto-Electronic Adv 2(11):190007–10. https://doi.org/10.29026/oea.2019.190007
4. Fan X, White IM (2011) Optofluidic microsystems for chemical and biological analysis. Nat Photonics 5(10):591–597. https://doi.org/10.1038/nphoton.2011.206
5. Psaltis D, Quake SR, Yang C (2006) Developing optofluidic technology through the fusion of microfluidics and optics. Nature 442(7101):381–386. https://doi.org/10.1038/nature05060
6. Asplund MC, Johnson JA, Patterson JE (2019) The 2018 Nobel Prize in Physics: optical tweezers and chirped pulse amplification. Anal Bioanal Chem 411(20):5001–5005. https://doi.org/10.1007/s00216-019-01913-z
7. Ashkin A, Dziedzic JM (1987) Optical trapping and manipulation of viruses and bacteria. Science 235(4795):1517–1520. https://doi.org/10.1126/science.3547653
8. Grigorenko AN, Roberts NW, Dickinson MR, Zhang Y (2008) Nanometric optical tweezers based on nanostructured substrates. Nat Photonics 2(6):365–370. https://doi.org/10.1038/nphoton.2008.78
9. Dholakia K, Čižmár T (2011) Shaping the future of manipulation. Nat Photonics 5(6):335–342. https://doi.org/10.1038/nphoton.2011.80
10. Gerena E, Legendre F, Molawade A, Vitry Y, Régnier S, Haliyo S (2019) Tele-robotic platform for dexterous optical single-cell manipulation. Micromachines 10(10):677
11. Ashkin A (1992) Forces of a single-beam gradient laser trap on a dielectric sphere in the ray optics regime. Biophys J 61(2):569
12. Zhang H, Liu K-K (2008) Optical tweezers for single cells. J R Soc Interface 5(24):671–690
13. Stout AL (2001) Detection and characterization of individual intermolecular bonds using optical tweezers. Biophys J 80(6):2976–2986
14. Raucher D, Sheetz MP (1999) Characteristics of a membrane reservoir buffering membrane tension. Biophys J 77(4):1992–2002
15. Yin M, Gerena E, Pacoret C, Haliyo S, Régnier S (2017) High-bandwidth 3d force feedback optical tweezers for interactive bio-manipulation. In: 2017 IEEE/RSJ International conference on intelligent robots and systems (IROS). IEEE, pp 1889–1894
16. Gerena E, Legendre F, Vitry Y, Regnier S, Haliyo S (2020) Improving optical micromanipulation with force-feedback bilateral coupling. In: 2020 IEEE International conference on robotics and automation (ICRA). IEEE, pp 10292–10298
17. Wu W, Zhu X, Zuo Y, Liang L, Zhang S, Zhang X, Yang Y (2016) Precise sorting of gold nanoparticles in a flowing system. ACS Photonics 3(12):2497–2504. https://doi.org/10.1021/acsphotonics.6b00737
18. Lasnoy E, Wagner O, Edri E, Shpaisman H (2019) Drag controlled formation of polymeric colloids with optical traps. Lab Chip 19(20):3543–3551. https://doi.org/10.1039/C9LC00672A
19. Geonzon LC, Kobayashi M, Sugimoto T, Adachi Y (2023) Adsorption kinetics of polyacrylamide-based polyelectrolyte onto a single silica particle studied using microfluidics and optical tweezers. J Colloid Interface Sci 630:846–854. https://doi.org/10.1016/j.jcis.2022.10.067
20. Wang MM, Tu E, Raymond DE, Yang JM, Zhang H, Hagen N, Dees B, Mercer EM, Forster AH, Kariv I, Marchand PJ, Butler WF (2005) Microfluidic sorting of mammalian cells by optical force switching. Nat Biotechnol 23(1):83–87. https://doi.org/10.1038/nbt1050
21. Zhu Y, You M, Shi Y, Huang H, Wei Z, He T, Xiong S, Wang Z, Cheng X (2023) Optofluidic tweezers: efficient and Versatile Micro/Nano-Manipulation tools. Micromachines 14(7):1326. https://doi.org/10.3390/mi14071326
22. Chowdhury S, Svec P, Wang C, Seale KT, Wikswo JP, Losert W, Gupta SK (2013) Automated cell transport in optical tweezers-assisted microfluidic chambers. IEEE Trans Autom Sci Eng 10(4):980–989. https://doi.org/10.1109/TASE.2013.2239287
23. Boodhun N (2018) Seeing is believing: structures and functions of biological molecules. Biotechniques 64(4):143–146. https://doi.org/10.2144/btn-2017-0123
24. Curtis JE, Koss BA, Grier DG (2002) Dynamic holographic optical tweezers. Optics communications 207(1–6):169–175
25. Gerena E, Régnier S, Haliyo S (2019) High-bandwidth 3-d multitrap actuation technique for 6-dof real-time control of optical robots. IEEE Robotics and Automation Letters 4(2):647–654
26. Roure OD, Saez A, Buguin A, Austin RH, Chavrier P, Siberzan P, Ladoux B (2005) Force mapping in epithelial cell migration. Proc Natl Acad Sci USA 102(7):2390–2395. https://doi.org/10.1073/pnas.0408482102
27. Charati SG, Stern SA (1998) Diffusion of gases in silicone polymers: molecular dynamics simulations. Macromolecules 31(16):5529–5535. https://doi.org/10.1021/ma980387e
28. Leclerc E, Sakai Y, Fujii T (2024) Cell culture in 3-dimensional microfluidic structure of PDMS (polydimethylsiloxane)
29. Wang C-Y, Bochkovskiy A, Liao H-YM (2022) YOLOv7: trainable bag-of-freebies sets new state-of-the-art for real-time object detectors. arXiv preprint arXiv:2207.02696
30. Ashkin A (1992) Forces of a single-beam gradient laser trap on a dielectric sphere in the ray optics regime. Biophys J 61(2):569–582. https://doi.org/10.1016/S0006-3495(92)81860-X
31. Simmons RM, Finer JT, Chu S, Spudich JA (1996) Quantitative measurements of force and displacement using an optical trap. Biophys J 70(4):1813–1822
32. Mukhopadhyay R (2007) When PDMS isn't the best. Anal Chem 79(9):3248–3253. https://doi.org/10.1021/ac071903e
33. Toepke MW, Beebe DJ (2006) PDMS absorption of small molecules and consequences in microfluidic applications. Lab Chip 6(12):484. https://doi.org/10.1039/b612140c